Bull Earthquake Eng (2015) 13:459–482
DOI 10.1007/s10518-014-9631-z

ORIGINAL RESEARCH PAPER

Elastic and inelastic systems under near-fault seismic shaking: acceleration records versus optimally-fitted wavelets

E. Garini · N. Makris · G. Gazetas

Received: 15 September 2013 / Accepted: 14 May 2014 / Published online: 3 June 2014

Abstract Four idealised dynamic systems, which are used as analogues in earthquake and geotechnical engineering, are studied: an elastic single-degree-of-freedom (sdof) oscillator; an elastic–perfectly-plastic sdof oscillator; a rigid block resting in simple frictional contact on a horizontal base; and a rigid block resting on a sloping plane. They are subjected to several near-fault-recorded ground motions bearing the effects of 'forward-rupture directivity' and fault surface dislocation ('fling-step') phenomena—long-period acceleration pulses and large velocity or displacement steps. Two types of idealized wavelets (the Mavroeidis & Papageorgiou and the Ricker wavelets) are optimally-fitted to each record, applying the matching procedure presented by Vassiliou and Makris (Bull Seismol Soc Am 101(2):596–618, 2011). Extensive comparisons between the accelerogram response and the corresponding-fitted wavelets response show if and when the destructive pulse-like part of the records is indeed their most deleterious component, and if and when this destructiveness can be captured with the particular fitted wavelets. For the two purely inelastic systems, in particular, the comparison elucidates the role of the contained pulses in the size of sliding displacements. The results reveal that while the response of elastic and elasto-plastic sdof systems to the wavelets is usually reasonably similar with the response to the actual records, this is not usually the case for the two purely inelastic (sliding) systems. The unpredictable consequences of seismic shaking on such systems, even if the shaking intensity and frequency content were precisely known, is best demonstrated with the sensitivity of the size of sliding displacement to the polarity (+ or −), the sequence and number of cycles, and even the details of the excitation.

Keywords Directivity · Fling · Newmark sliding · Single degree of freedom oscillator · Elastic spectra · Elasto-plastic spectra · Sliding spectra · Wavelet analysis

E. Garini · G. Gazetas (✉)
National Technical University of Athens, Athens, Greece
e-mail: gazetas@ath.forthnet.gr

N. Makris
University of Patras, Patra, Greece

List of symbols

A_C	Critical yielding acceleration of the block
$A(t)$, A_H	Acceleration time-history, and maximum acceleration
$D(t)$, D	Sliding displacement time-history, and maximum sliding displacement
D_{res}	Residual (permanent) displacement
$D_{M\&P}$	Maximum sliding displacement induced by the Mavroeidis & Papageorgiou wavelet
D_{RICKER}	Maximum sliding displacement induced by the Ricker wavelet
pI	Pulse indicator (Vassiliou and Makris 2011)
s	A scale parameter that controls the dilation/contraction of the wavelet
S_A	Response spectral acceleration
T	The period of a single degree of freedom oscillator
$V(t)$	Ground velocity time-history
ΔV	Velocity step
γ	A parameter that controls the oscillation character of the wavelet
β	Angle of the inclined plane measured from the horizontal
ζ	Damping ratio
ξ	Translation time of wavelet
φ	Wavelet's phase angle
τ	Time duration of a pulse
k	Stiffness
μ_F	Coulomb's constant coefficient of friction
μ_{str}	Ductility (ratio of *total elastic plus plastic* over elastic displacement)

1 Introduction: The nature of near-fault ground motions

Near-fault ground motions of major seismic events usually contain severe 'directivity' and 'fling' pulses. The former are the result of *coherently arriving seismic waves* whenever the fault ruptures towards the site—which is known as 'forward-rupture directivity' (Bolt 1976; Singh 1985; Somerville et al. 1996; Somerville 2000, 2003; Abrahamson 2001). Large permanent displacement of a record results from the *tectonic permanent offset* of the earth in the proximity of the seismogenic fault rupture—'*fling step*' (Abrahamson 2000; and Bolt 2004; Mavroeidis and Papageorgiou 2010).

Figure 1 portrays, with two selected seismic records as examples, some fundamental characteristics of near-fault motions. In case of a strike–slip earthquake (as sketched for example at the top of Fig. 1), the "signature" of forward rupture directivity appears in direction *normal* to the fault (record of JMA during the Kobe earthquake); whereas, the fling step is significant in the *parallel* component of motion in close proximity to the fault, especially if the latter emerges on the surface with a large static offset (Yarimca record, Kocaeli earthquake). Motions with *only* forward-directivity pulses terminate with no permanent displacement, as depicted with the JMA record (fault-normal component) of the 1995 Kobe (Japan) earthquake. The deeper nature of the two phenomena has been investigated analytically in a seminal paper by Hisada and Bielak (2003).

Such motions have the potential to inflict large irrecoverable deformations on structural and/or geotechnical systems, especially on those characterized by a plastic rather than elastic behaviour (Garini et al. 2011; Gazetas et al. 2009). The *ultimate* aim of this paper is to answer the question: how significant is the dominant large-duration pulses of a near-fault record for the damage that such a record may inflict on various types of structures. In other words, is

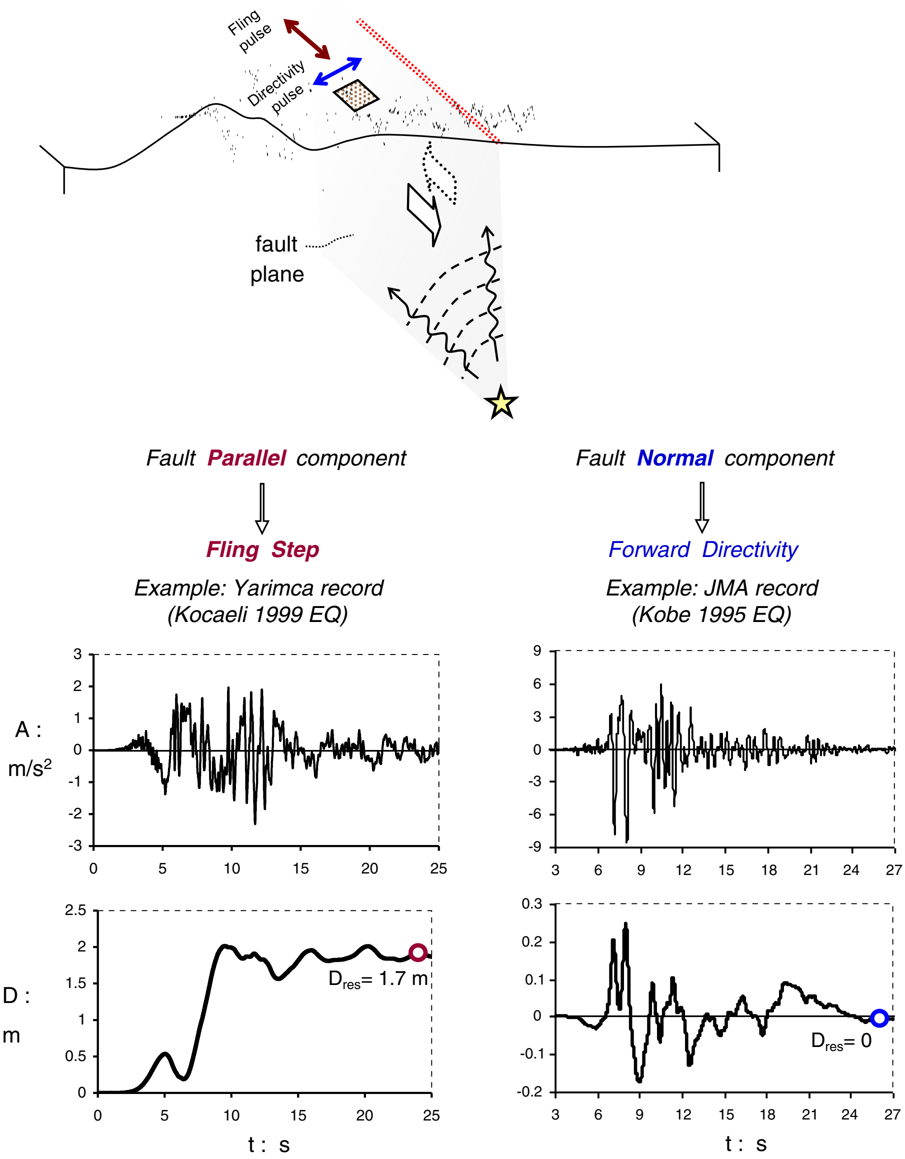

Fig. 1 Schematic explanation of the '*fling-step*' and '*forward-directivity*' phenomena as reflected in the two sets of acceleration and displacement time histories

it only this single, dominant pulse that causes the large displacement, or is it perhaps the whole sequence of pulses (which constitute a particular record) that play an equally or more significant role? To achieve this goal, eleven near-fault records (listed in Table 1) are used. To each record a single wavelet is "optimally" fitted by utilizing the method developed by Vassiliou and Makris (2009, 2011). Comparison of the responses due to the real motions and their corresponding wavelets sheds light on the unique significance of the near-fault pulses. It is emphasized however, that our conclusions strictly rely on the success of wavelet fitting on the actual accelerograms.

Table 1 List of near-fault earthquake records utilized as excitations in this study

Earthquake, magnitude	Record name	pga (g)	pgv (m/s)	pgd (m)
Kobe—Japan, $M_W = 7.0$ (16 *January* 1995)	*Fukiai*	0.763	1.232	0.134
	Takatori-0°	0.611	1.272	0.358
Northridge—California, $M_W = 6.8$ (17 *January* 1994)	*Newhall Firestation*-360°	0.589	0.753	0.182
	Rinaldi-228°	0.837	1.485	0.261
Chi-Chi Taiwan, $M_W = 7.5$ (20 *September* 1999)	*TCU* 052-*EW*	0.350	1.743	4.659
	TCU 068-*NS*	0.353	2.892	8.911
Kocaeli—Turkey, $M_W = 7.4$ (17 *August* 1999)	*Sakarya*-EW	0.330	0.814	2.110
	Yarimca-60°	0.231	0.906	1.981
Duzce—Turkey, $M_W = 7.2$ (12 *November* 1999)	*Duzce*-270°	0.535	0.835	0.516
Christchurch—New Zealand, $M_W = 6.3$ (24 *February* 2011)	*CCCC-N64E*	0.473	0.710	0.215
	REHS-S88E	0.713	0.874	0.271

2 Approximating accelerograms with best-fitted wavelets

The selected near-fault motions are used as base excitations from each of which two wavelets are "extracted": (i) a Ricker wavelet and (ii) a Mavroeidis and Papageorgiou (2003) wavelet. The method of wavelet analysis introduced by Vassiliou and Makris (2009, 2011) is used for the wavelet fitting. Their optimization process attempts to capture the major near-fault pulses of the motions, not the details. Then each of the 11 near-fault accelerograms (shown in Fig. 2) and their corresponding 22 idealized *wavelets* excite the four fundamental systems (of Fig. 3).

Elastic and elastoplastic acceleration spectra for the simple (sdof) oscillator and sliding spectra for the symmetric and asymmetric rigid-plastic systems represent the consequences of the near-fault motions. The agreement or disagreement between these spectra of the actual records and those of their wavelet approximations is investigated. Detailed time-histories of the sliding response are examined to develop a deeper understanding of the phenomena involved.

A list of "severe" near-fault records utilized in our study, is given in Table 1 along with their peak parameters. The term "severe", is meant to emphasize the selection of near-fault motions that contain "deleterious" pulses: either of large duration, or of high-amplitude, or of both. The selection was among the records with the strongest (not the average) near-fault effects.

In the Vassiliou and Makris (2009, 2011) wavelet fitting procedure "energetic" acceleration pulses and their associated frequency and amplitude are extracted from a record in the form of fitted wavelets. Their approach extended the standard wavelet transform to a more general transform, by incorporating a phase modulation together with a cycle number and symmetry manipulation to the already typical functions (wavelet translation and dilation–contraction) of the standard wavelet transform.

In brief, the extended wavelet transform is defined as:

$$C(s,\xi,\gamma,\varphi) = w(s,\gamma,\varphi)\int_{-\infty}^{\infty} A(t)\cdot\psi\left(\frac{t-\xi}{s},\gamma,\varphi\right)dt \tag{1}$$

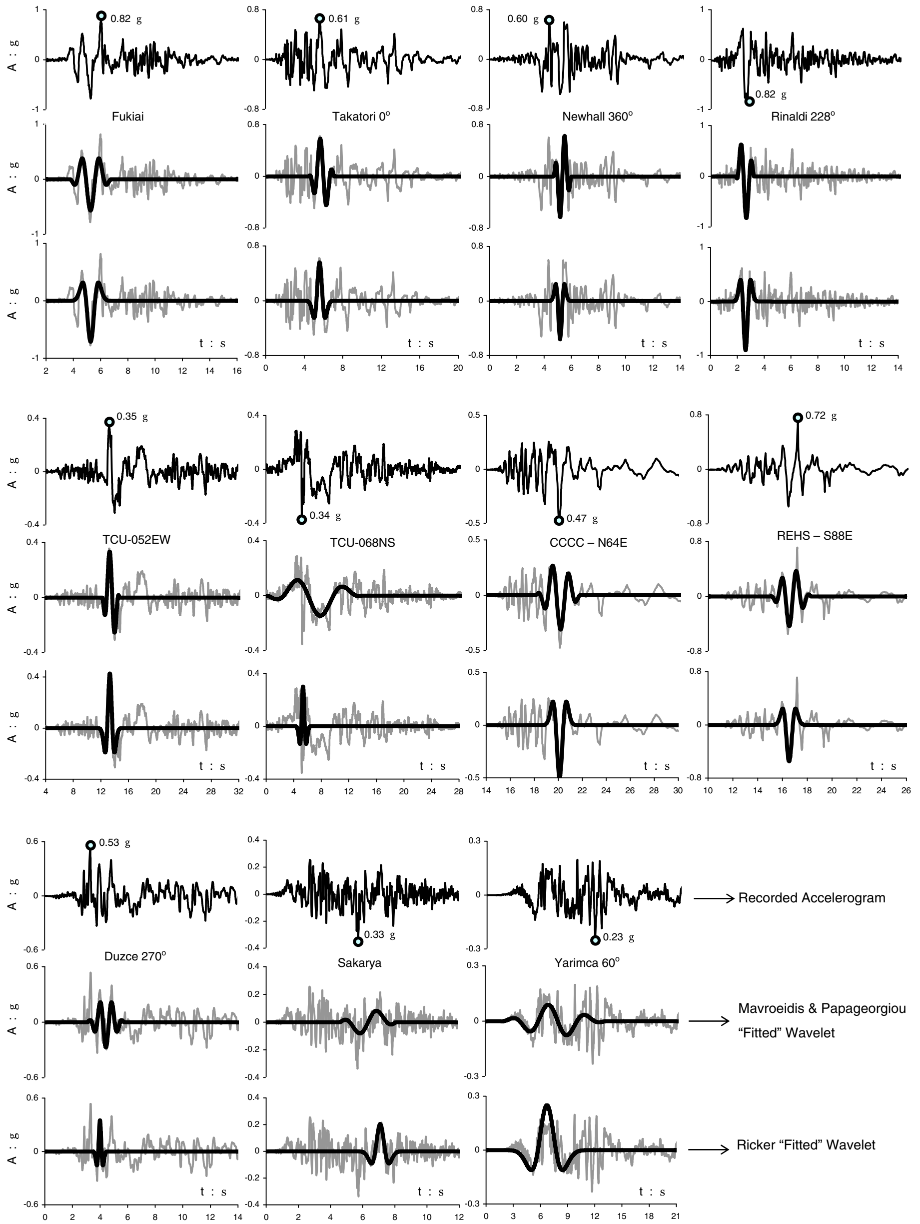

Fig. 2 Acceleration time histories of the utilized excitations in terms of actual recordings, and of their fitted M&P and Ricker wavelets

where s is the scale parameter that controls the dilation or contraction of the wavelet, ξ is the translation time (thus the movement of the wavelet along the time axis), γ is a parameter that controls the oscillatory nature of the signal, φ is the phase angle, $\psi(t, s, \xi, \gamma, \varphi)$ is the wavelet function, and $A(t)$ is the acceleration time history. The quantity $w(s, \gamma, \varphi)$ outside the integral in Eq. (1) is a weighting function. For the purposes of this study, $w(s, \gamma, \varphi)$ is formed to ensure that all wavelets at every scale s have the same energy. In particular, for

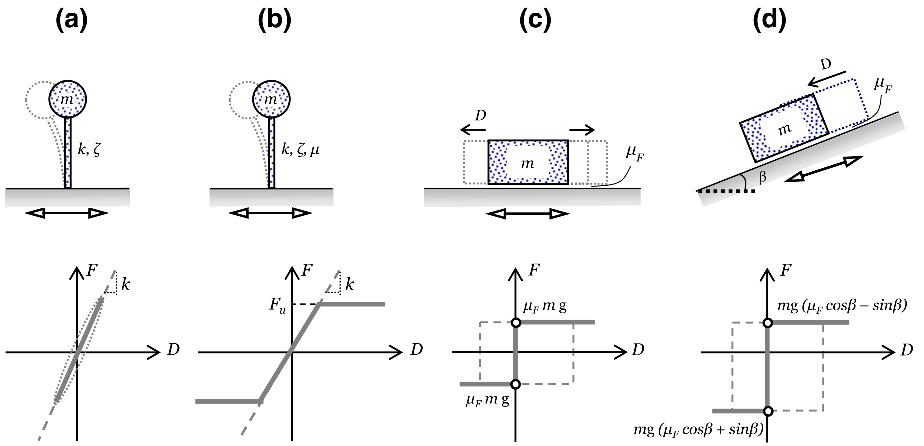

Fig. 3 The fundamental systems ("analogues") studied in the paper with their restoring force-displacement or moment–rotation relations: **a** visco-elastic oscillator; **b** elasto-plastic oscillator; **c** ideally rigid-plastic sliding on a horizontal plane; and **d** ideally rigid-plastic sliding on an inclined plane. μ_F = coefficient of friction, μ = ductility = plastic over elastic displacement ratio

the Mavroeidis & Papageorgiou (M&P) wavelet the weighting function $w(s, \gamma, \varphi)$ is equal to:

$$w\,(s, \gamma, \varphi) = \frac{1}{\sqrt{\frac{1}{8}s\left[2\gamma + 6\gamma^3 + \frac{\cos(2\varphi)\cdot\sin(2\pi\gamma)}{\pi(1-4\gamma^2)}\right]}} \tag{2}$$

The full mathematical definition and properties of this extended wavelet transform are presented in the paper of Vassiliou and Makris (2009, 2011).

Two types of wavelets are employed in this study:

- The symmetric Ricker wavelet (2nd derivative of Gaussian, also called "Mexican Hat"):

$$\psi\left(\frac{t-\xi}{s}\right) = \left[1 - \left(\frac{t-\xi}{s}\right)^2\right]\exp\left[-\frac{1}{2}\left(\frac{t-\xi}{s}\right)^2\right] \tag{3}$$

- The general M&P wavelet (2003):

$$\psi\left(\frac{t-\xi}{s}, \gamma, \varphi\right) = \left[\sin\left(\frac{2\pi}{s\gamma}(t-\xi)\right)\cos\left(\frac{2\pi}{s}(t-\xi)+\varphi\right)+\gamma\sin\left(\frac{2\pi}{s}(t-\xi)+\varphi\right)\right]\cdot \left[1+\cos\left(\frac{2\pi}{s\gamma}(t-\xi)\right)\right] \tag{4}$$

Recall that the latter wavelet derives from the Gabor wavelet by replacing the Gaussian envelope with a cosine function. Thanks to its polyparametric nature, the M&P wavelet can be either symmetric or asymmetric depending on the exact shape of the targeted section of the record (Mavroeidis and Papageorgiou 2010). And it also has a number of cycles as needed for a close fit.

Our choice of (only) these two types of wavelets is based on the quantitative evaluation of seven wavelets presented by Vassiliou and Makris (2009, 2011). For a wide number of records, Vassiliou & Makris investigated the matching ability of seven wavelets and concluded that the M&P wavelet attained the highest score—hence our selection. However, a symmetric wavelet, like the Ricker pulse expressed by Eq. (3), seemed a decent representative of less severe "more typical" wavelets—thus our second choice.

The dual scope of this paper is to examine the level of success of the fitted wavelets to predict the elastic, elastoplastic, and rigid-plastic response induced by the real accelerograms; and in the process to evaluate the significance of the dominant pulses on the response. Previous studies that also examine the elastic and inelastic response triggered by near-fault motions when approximated with pulselike wavelets, are presented by Makris and Black (2004a,b,c), Makris and Psychogios (2006), and Karavasilis et al. (2010). However, in these studies the emphasis is given to the structural response of single- and multi-story steel moment resisting frames.

The selected accelerograms (listed in Table 1) and the corresponding pairs of fitted wavelets are shown superimposed in the plots of Fig. 2. Notice the flexibility of M&P wavelet and its capability to achieve an intensely asymmetric shape, for example in the Takatori, Newhall and Rinaldi records.

3 The fundamental elastic and inelastic analogues

The four fundamental analogues of Fig. 3 represent in generic form some fundamental structural and geotechnical systems, and include: the single degree of freedom (sdof) elastic oscillator (of mass m, stiffness k, and damping coefficient ζ), the sdof elastic–perfectly-plastic oscillator whose restoring force is linear up to an ultimate capacity F_u and constant thereafter leading to an inelastic displacement expressed through its ductility, μ_{str} (the ratio of system's total elastoplastic over its elastic displacement). Several applications especially in geological and geotechnical engineering require understanding of dynamic sliding, represented here by a rigid block of mass m supported on seismically vibrating base. The case of symmetric friction is modelled with a block sliding on a horizontal base. The frictional resistance is $F = \pm\mu mg$, where μ is the (presumed *constant)* coefficient of Coulomb friction at the block–base interface. The analysis of the response of the block to motion $A(t)$ is a straightforward application of Newton's law of motion along with rigid-body kinematics. It is a process well understood and need not be further discussed. We will call critical acceleration, $A_C = \mu g$, the one beyond which slippage initiates.

For asymmetric friction the block rests on an inclined plane (angle β). The frictional resistance (for excitation acting parallel to the slope) is $F_1 = mg(\mu cos\beta - sin\beta)$ when the block slides downward, and $F_2 = mg(\mu cos\beta + sin\beta)$ when it slides upward. Therefore, the critical acceleration for downhill slippage is $A_{C1} = (\mu cos\beta - sin\beta)\ g$, and for uphill $A_{C2} = (\mu cos\beta + sin\beta)g$.

Thanks to the transient nature of earthquake loading $A(t)$, even if the base were to experience a number of acceleration pulses in the upward or downward direction higher than the critical values A_{C1} or $A_{C2,}$ this would only lead to *finite* sliding displacements downslope or upslope respectively. For small values of the angle β (for $\beta < 5°$), when A_{C2} is not much larger than A_{C1}, it is quite possible that slip may occur in both directions. But for larger angles, as is appropriate for natural slopes: $A_{C2} >> A_{C1}$ and sliding occurs only downhill—hence, the accumulated residual slip is simply the sum of the individual slip-steps.

The asymmetric sliding analogue, *a rigid block on inclined plane,* has numerous applications in geotechnical engineering: seismic performance of earth dams and embankments, gravity retaining walls, landslides, landfills with geosynthetic liners, and concrete gravity dams (Newmark 1965; Ambraseys and Sarma 1967; Makdisi and Seed 1978; Richards and Elms 1979; Sarma 1975, 1981; Lin and Whitman 1983; Wilson and Keefer 1983; Constantinou et al. 1984; Constantinou and Gazetas 1987; Ambraseys and Menu 1988; Leger and Katsouli 1989; Yegian et al. 1991; Gazetas and Uddin 1994; Harp and Jibson 1995; Fenves and Chopra 1986; Kramer 1996; Kramer and Smith 1997; Yegian et al. 1998; Bray and Rathje 1998; Crespellani et al. 1998; Rathje and Bray 1999; Sarma and Kourkoulis 2004).

In addition to the obvious use of the presented results in a number of real-life seismic structural and geotechnical problems, we think of the block-on-horizontal or inclined-plane model as representing systems with *strongly and purely inelastic* behavior. It will be shown that such systems are particularly sensitive to both 'directivity' and 'fling' related pulses—far more so than the elastic systems.

4 Structural response: analyses and comparisons

By wavelet matching of records, we intent to capture the most essential pulse-like characteristics of the original accelerogram. A way to quantify the effectiveness of this wavelet approximation is through the acceleration response spectrum—a frequency range representation of sdof elastic response. The next two figures address the response of a purely elastic (Fig. 4) or an elastic–perfectly-plastic oscillator (Fig. 5) in terms of response spectral acceleration, S_A, versus period, T. For each record, three acceleration response spectra curves are shown: for the original accelerogram (black line), for the corresponding M&P wavelet (bold grey line), and for the Ricker wavelet (bold black line).

As illustrated in Fig. 4, the agreement between the elastic spectra of the wavelets and the original motions is satisfactory in some cases and unsatisfactory in others. Specifically, for the accelerograms of TCU-052EW, Fukiai, Newhall 360°, Rinaldi 228°, CCCC-N64E and REHS-S88E, an almost surprisingly good agreement is achieved for the entire period range, despite the conspicuous differences in their time histories. The reason is that all these records exhibit distinctive, well-defined directivity and/or fling acceleration pulses which can be clearly detected and captured with the two types of wavelets. In stark contrast, with the TCU-068NS record while the Ricker response spectrum barely agrees with the original in the period range of 0.7–1.2 s and diverges widely at longer periods, the M&P spectrum matches the original in the long period range of 3.5–8 s but fails dramatically at shorter periods. The reason for this can be visualized in the comparison of Fig. 2 between the real and the fitted motions: the M&P wavelet captures the very long-duration fling-related pulses of the recorded motion between the 6 and 10 s, but completely ignores the short-duration peaks at t = 4–6 s. The Ricker wavelet does exactly the opposite.

For the elastoplastic 1-dof system, the sets of three acceleration spectra are given in Fig. 5. Here, the imposed ductility demand, $\mu_{str} = 2$, is defined as the ratio of the developing total (elastic plus plastic) displacement over the elastic displacement. The conclusions drawn for the elastic spectra in the previous paragraph are valid for the bilinear sdof system as well. Notice that the absolute values of spectral acceleration are roughly half of the elastic ones, as expected.

In conclusion, the elastic and moderately-inelastic response spectra of the Ricker and M&P wavelets are often but not always in broad agreement with the spectra of the original records.

5 Rigid-plastic systems: analyses and comparisons

The fundamental difference of the sdof oscillator from the sliding block systems stems from the inherent plasticity of the frictional behaviour, which dominates the response. It is

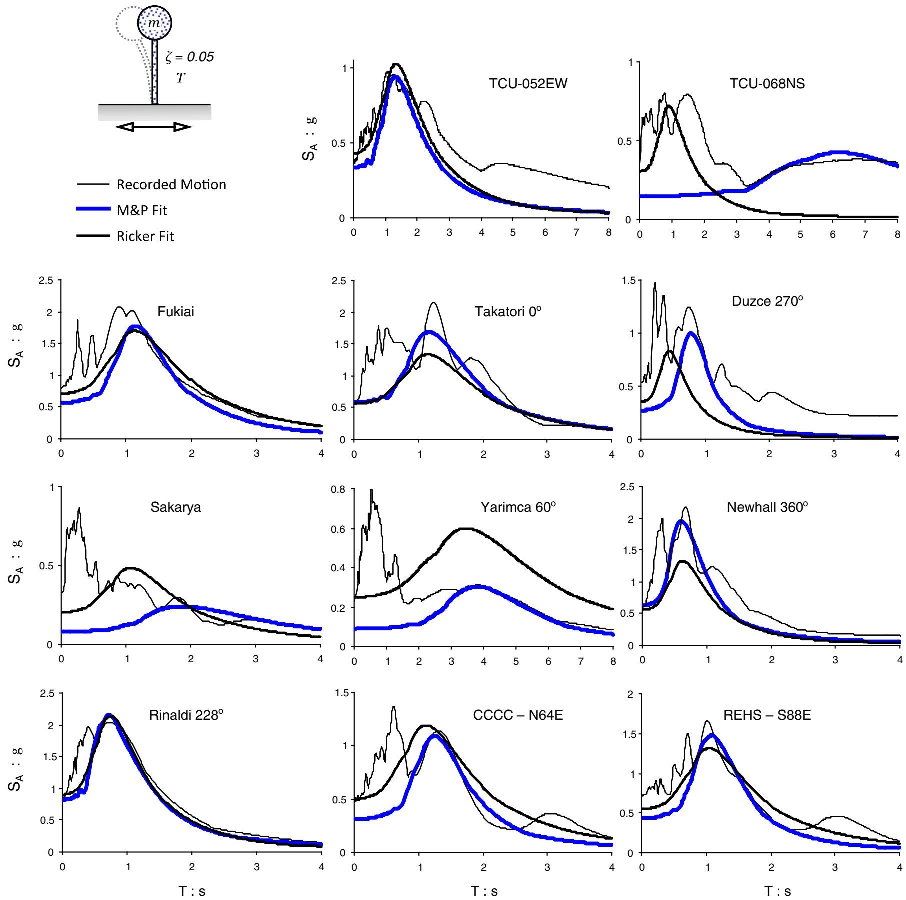

Fig. 4 Elastic acceleration spectra, S_A, of a single degree of freedom oscillator with damping ratio $\zeta = 5\,\%$. With the bold black line is illustrated the response triggered by the Ricker fitted wavelet, whereas with the bold grey line the response of the M&P wavelet fit. Both are compared with the acceleration response induced by the original record

interesting to see whether the sliding displacements are influenced by the details of the input motion, in other words if the sequence of acceleration cycles omitted in the wavelet fitting process affect the slippage and to what extent. A limited number of analyses are shown here in detail (Figs. 6, 7, 8, 9, 10, 11, 12, 13), but the results of all analyses are compiled in Fig. 14 to offer a complete overview.

Figure 6 compares the sliding behavior of a mass on a horizontal plane shaken by: (i) the fling-step—affected Yarimca accelerogram (recorded close to the Anatolia fault which ruptured about 3 km away in the Kocaeli 1999 earthquake), and (ii) the fitted M&P wavelet. The sliding response is presented in terms of acceleration, velocity and slippage time-histories. The critical acceleration of the block is chosen as $A_C = 0.05$ g (i.e., coefficient of friction 0.05), meaning that no higher acceleration can be transmitted to the block. The 60°-component of the Yarimca record exhibits a peak ground acceleration of merely 0.23 g. However, as indicated in Fig. 6, it attains a significant velocity pulse with duration ≈4.3 s and a velocity step $\Delta V \approx 1.33$ m/s—such velocity characteristics bear the signature of

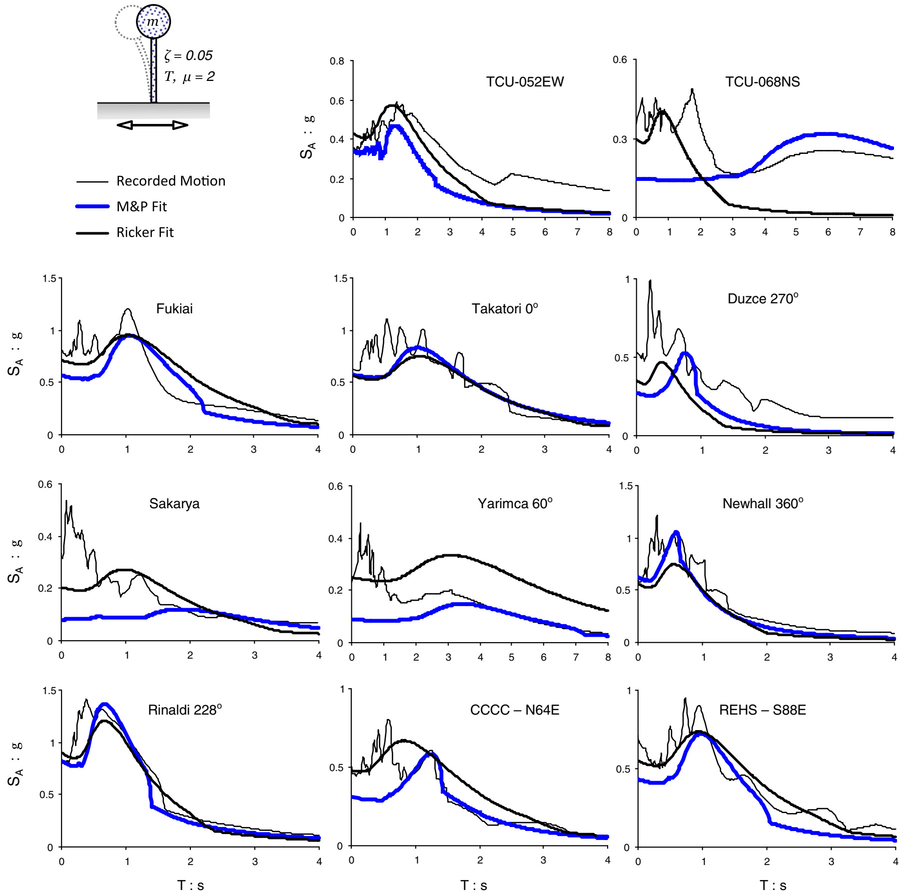

Fig. 5 Inelastic acceleration spectra, S_A, of a single degree of freedom oscillator with plasticity index $\mu_{str} = 2$, and damping ratio $\zeta = 5\,\%$. With the *bold black line* is illustrated the response triggered by the Ricker fitted wavelet, whereas with the *bold grey line* the response of the M&P wavelet fit. Both are compared with the acceleration response induced by the original record

both forward-rupture directivity and of fling step. As a result, the peak sliding displacement reaches 0.41 m. When 'Yarimca' is approximated with the M&P wavelet (right handside of Fig. 6), the maximum slippage drops only slightly to 0.36 m—unsurprisingly, since this wavelet matches faithfully the velocity of the original pulse. The duration of the velocity pulse from 4.30 s (in the original) increases to 4.90 s (in the wavelet), but the velocity step from the original 1.33 m/s drops to 1.17 m/s. Therefore, this wavelet captures the essential characteristics of the excitation (same impulse $\Delta V \times \tau$, where τ is the pulse duration), leading to similar maximum slippage. Notice that the discussed figure refers to the smallest critical acceleration $A_C = 0.05$ g. However, we expect the same good or bad convergence between fitted and actual slippage to be more-or-less valid for larger values of A_C. Because as the yielding acceleration increases the details of the accelerogram play a less important role, and hence it is the major acceleration pulses that dominate the behaviour. Therefore the fitted pulses (which indeed approximate the major acceleration pulses) result in slippage closer to the actual one.

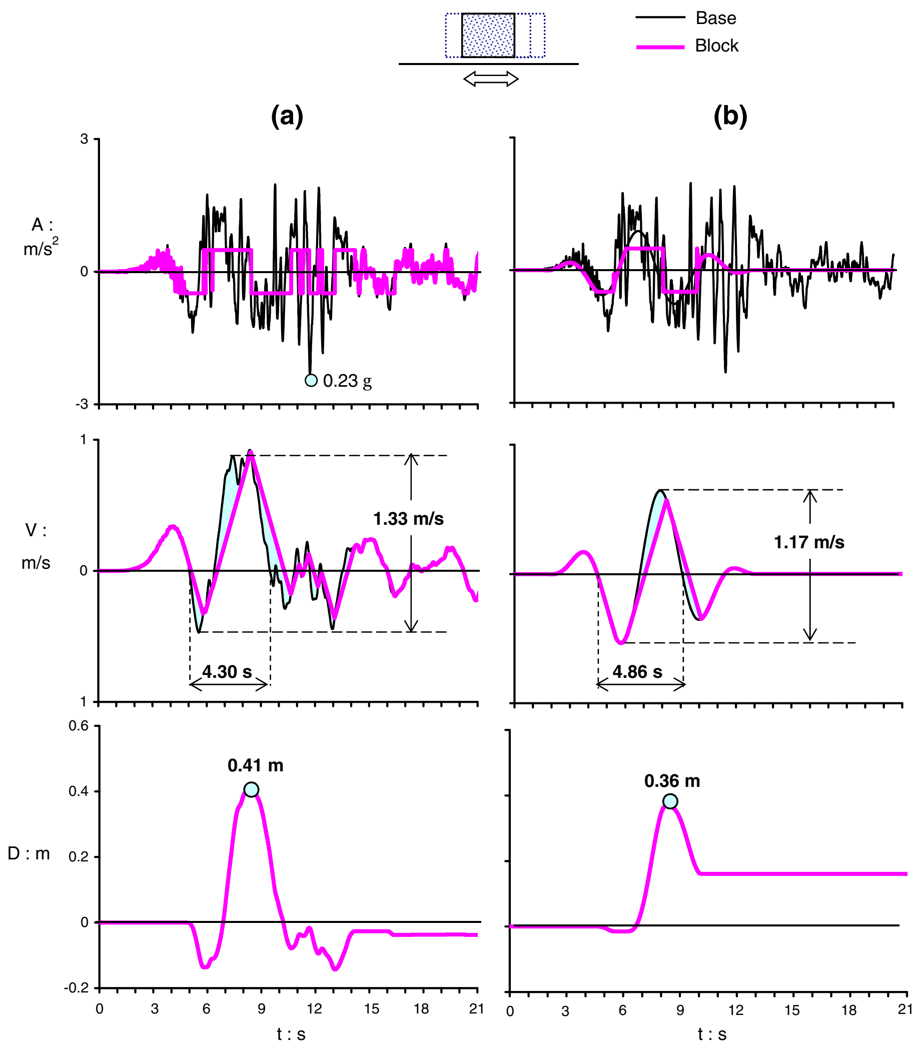

Fig. 6 Acceleration, velocity and sliding displacement (block minus base displacement) time histories induced by: **a** the Yarimca-60° ground motion, and **b** the fitted M&P wavelet to this motion ($A_C = 0.05$ g, $\beta = 0°$)

Now, would a similarly good agreement be true for asymmetric sliding?

As illustrated in detail in Fig. 7, the final slippage of the block on top of a 25° sloping plane subjected to the Yarimca record reaches 0.83 m, whereas the M&P fitted wavelet leads to merely 0.38 m. One of the causes is evident in the velocity time-histories: the first sliding period starting at 6 s until 8.6 s is similar in the original record and the M&P wavelet; but the following velocity sequence of pulses after t = 9 s, while present in the original record, is missing from the fitted wavelet. Hence, a total of five additional sliding events after the first major one occur with the Yarimca record (see left handside of Fig. 7), leading to a total slippage accumulation of 0.83 m. Of course, the velocity peak of the wavelet is some 30 % smaller than the real peak, causing an underestimation of the first major slippage from about 0.55–0.38 m.

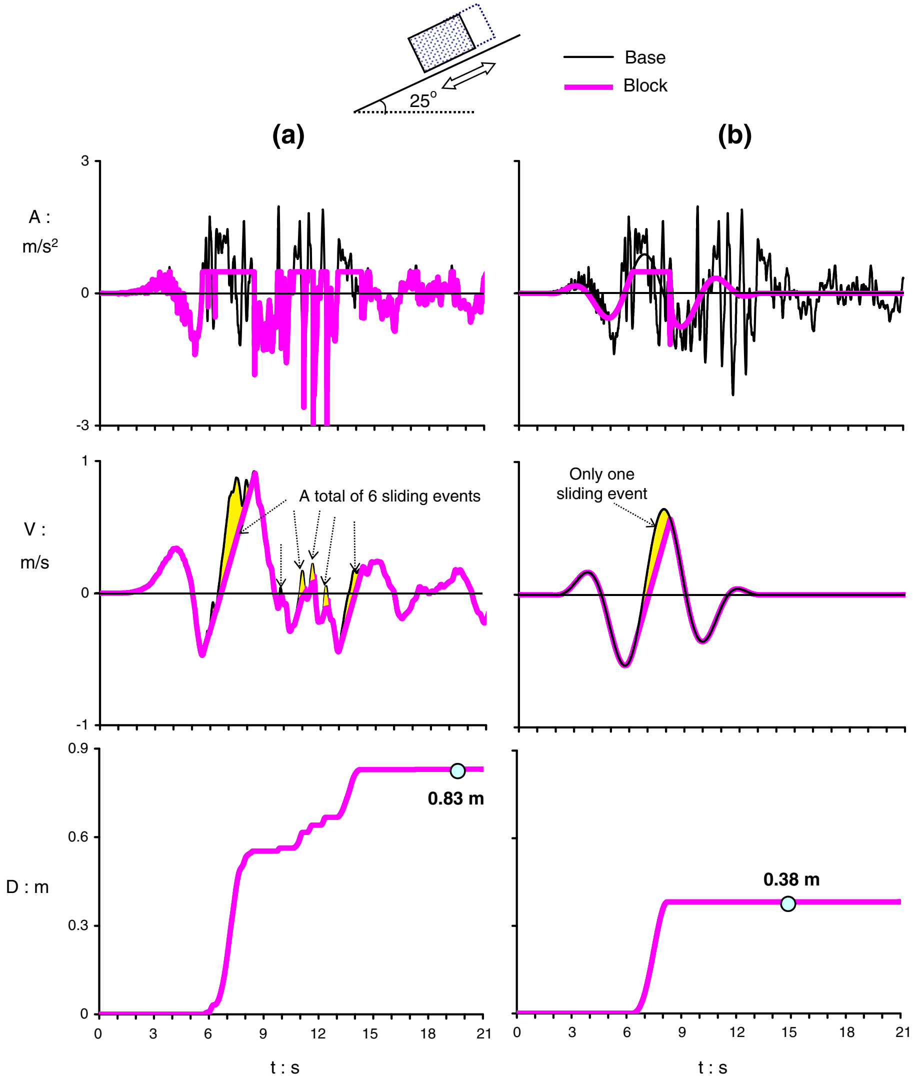

Fig. 7 Acceleration, velocity and sliding displacement (block minus base displacement) time histories induced by: **a** the Yarimca-60° ground motion, and **b** the fitted M&P wavelet to this motion ($A_C = 0.05$ g, $\beta = 25°$)

A complete presentation of the symmetric sliding response to the Takatori ground motion (component 0° of the 1995 Kobe earthquake and its fitted wavelets is illustrated in Fig. 8 for five values of the critical sliding acceleration A_C (0.05, 0.1, 0.2, 0.3, and 0.4 g). Notice that while the fit of both wavelets is very poor for critical accelerations up to 0.2 g, the fit significantly improves for higher values of A_C. The explanation is straightforward: for A_C values smaller than 0.2 g a large number of acceleration cycles in the original motion induce sliding of the rigid body, whereas for A_C larger than 0.2 g the slippage is mainly triggered by the large-period acceleration pulse at around 6 s. With the Ricker and M&P pulses we approximate adequately this large-period pulse, while all the rest acceleration details are neglected. Therefore, for $A_C > 0.2$ g the response of the fitted wavelets are closer to the

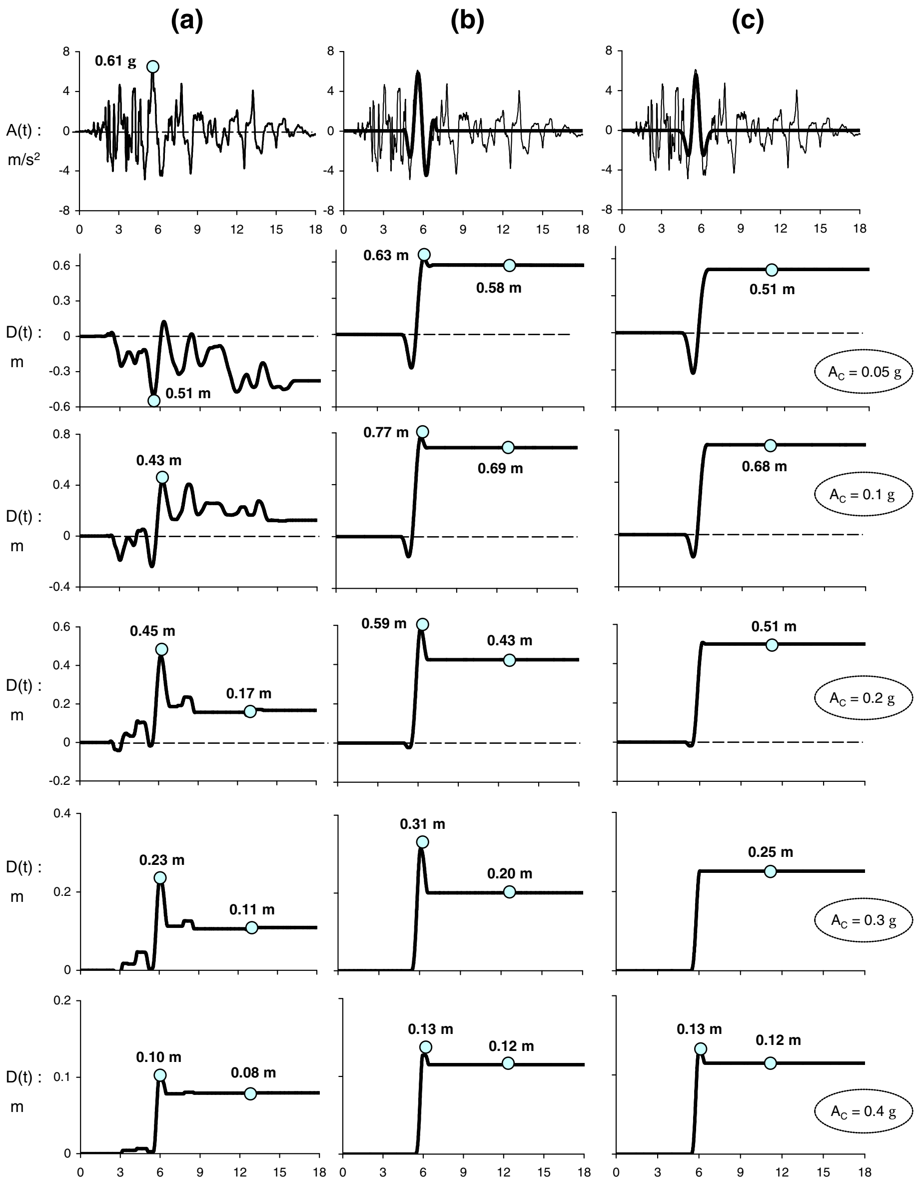

Fig. 8 Slippage time histories of a block on a *horizontal plane* induced by: **a** the Takatori-0° ground motion, **b** the fitted M&P wavelet; and **c** the fitted Ricker wavelet. The six rows are for the three acceleration time-histories and the induced slippage for five different critical accelerations ($A_C = 0.05{-}0.4$ g; smallest on *top*)

actual one. However, the acceleration pulse sequence of each particular ground motion is unique, so we could not draw a single upper "limit" of A_C after which the fitted wavelets could estimate reliably slippage.

Figures 9, 10 and 11 show the symmetric and asymmetric sliding response triggered by the Rinaldi motion (component 228°) recorded in the Northridge (1994) event. Rinaldi is a most characteristic forward-rupture directivity affected motion: a long–duration, high–

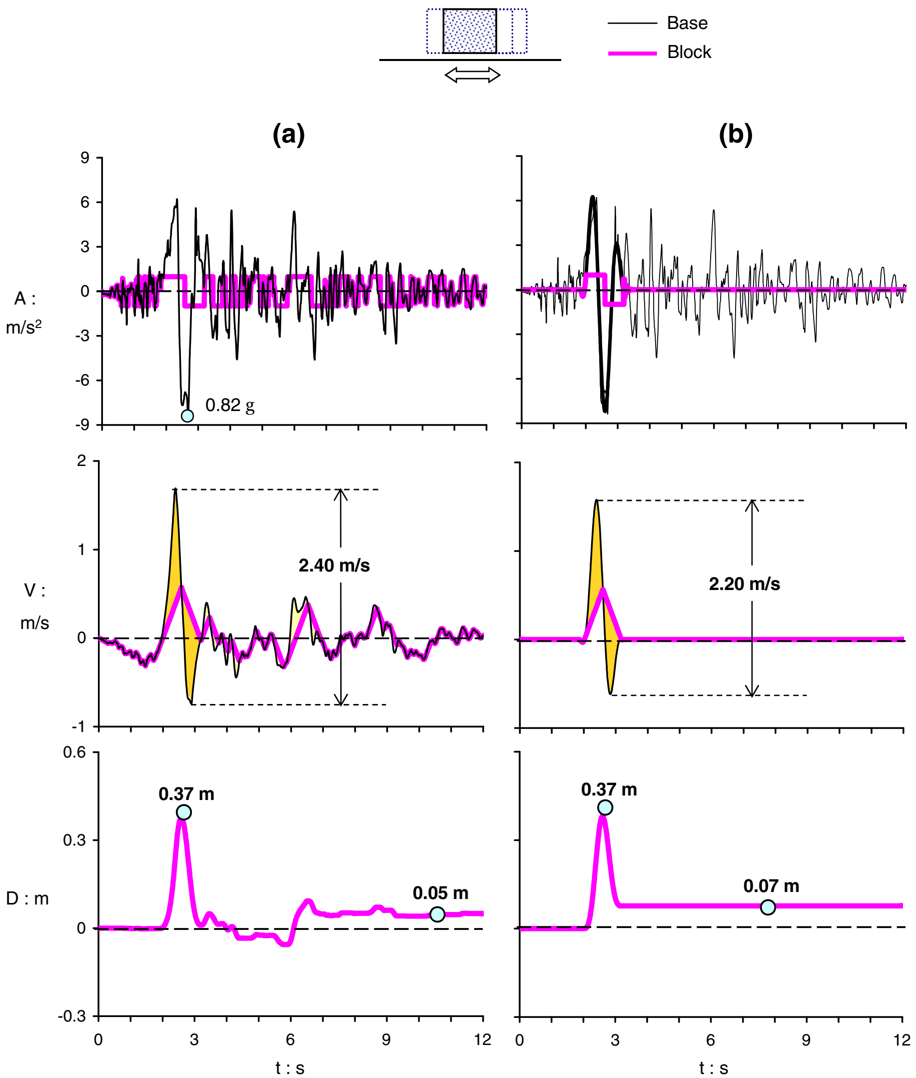

Fig. 9 Acceleration, velocity and sliding displacement (block-base displacement) time histories induced by: **a** the Rinaldi-228° ground motion, and **b** the fitted M&P wavelet to this motion ($A_C = 0.10$ g, $\beta = 0°$)

amplitude acceleration cycle (starting at about 2 s until 4 s, with an absolute peak amplitude of 0.82 g) prevails—apparently the result of superposition of "simultaneously" arriving seismic waves from the fault rupturing towards the site (Bertero et al. 1978; Somerville et al. 1996, 1997; Abrahamson 2000, 2001; Somerville 2000, 2003). The potential to inflict damage of this acceleration cycle is revealed in the velocity time history: a substantial velocity step $\Delta V = 2.40$ m/s. Yet, for a critical sliding acceleration $A_C = 0.10$ g, Rinaldi induces a peak slippage of merely 0.37 m and an insignificant permanent displacement of 0.05 m (left handside of Fig. 9). This peak slippage of 0.37 m, due entirely to the major directivity cycle, is perfectly matched by the M&P wavelet despite its somewhat smaller velocity step (2.17 m/s instead of 2.40 m/s).

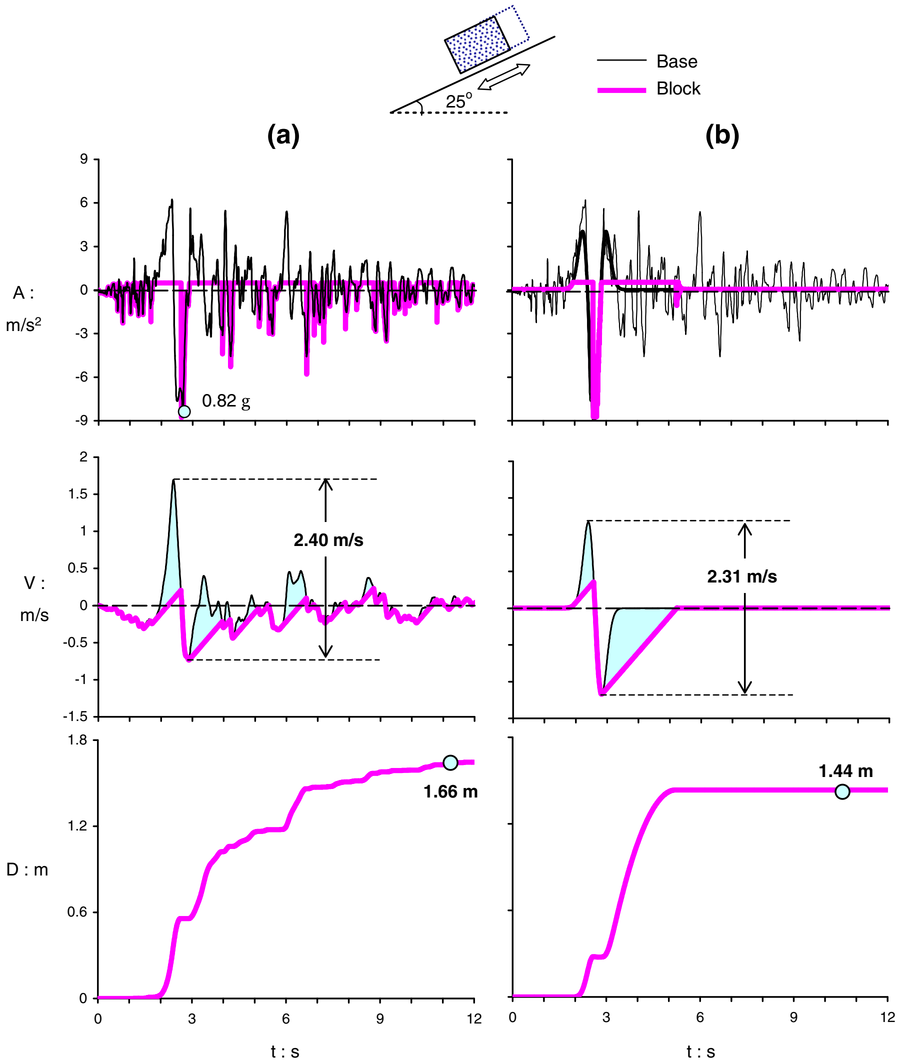

Fig. 10 Acceleration, velocity and sliding displacement time histories induced by: **a** the Rinaldi-228° ground motion, and **b** the fitted Ricker wavelet ($A_C = 0.05$ g, $\beta = 25°$)

The same trend is noticed for sliding on an inclined plane, as pictured in Fig. 10. The Rinaldi record is now approximated by a Ricker wavelet which leads to an accumulated slippage amounting to 1.44 m, barely missing the "target" of 1.66 m of the complete record.

However, another important aspect of asymmetric sliding is the polarity effect—the effect of reversing a motion's sign. A geotechnical analogue related to polarity is the dynamic response of two *identical* slopes located "*across the street*" and hence subjected to the same excitation (see sketch in Fig. 12). In the particular case of Rinaldi as shown in Fig. 11, the influence of polarity on slippage is enormous: reversal of excitation doubles the sliding response. Evidently, 'directivity' and 'fling' pulses of near-fault strong motions are inherently asymmetric, thereby aggravating the asymmetry of the slippage on inclined base. The reader

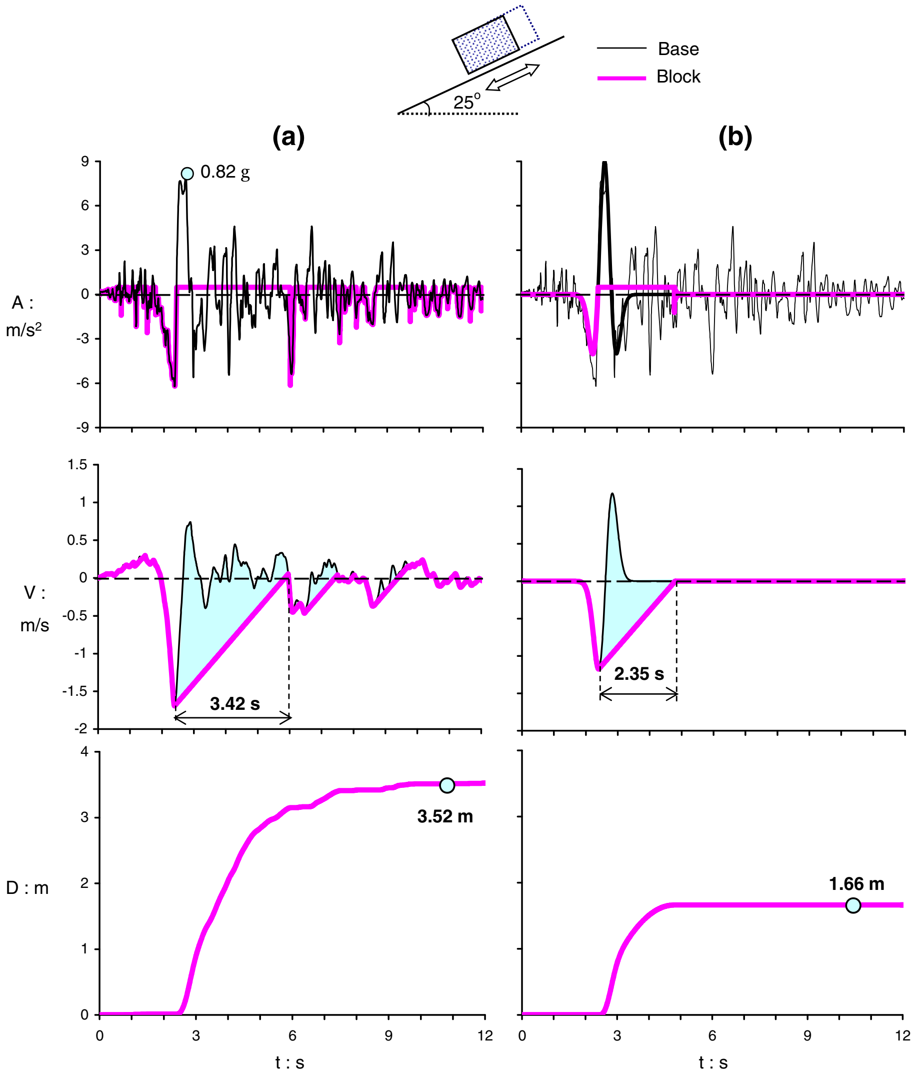

Fig. 11 The polarity effect: acceleration, velocity and sliding displacement time histories induced by: **a** the reversed Rinaldi-228° ground motion, and **b** the fitted Ricker wavelet ($A_C = 0.05$ g, $\beta = 25°$)

can appreciate the fact that regardless of the + or − sign a record has a single elastic response spectrum, and a single Arias Intensity, Housner Intensity, etc. But the induced sliding displacements are quite different.

Figure 12 portrays the asymmetric sliding spectra induced by: (a) the Rinaldi record when imposed with the two polarities—hence the two thin black curves; (b) the fitted M&P wavelet also with two polarities—the two bold grey curves; and (c) the fitted Ricker pulse with two polarities—the two bold black lines. As expected, good agreement between the slippage due to the record and the two matching wavelets is obtained for large values of critical yielding acceleration A_C, and hence small values of slippage (moderate inelasticity). For small values of A_C (i.e. for strongly inelastic systems) the disparity between the six curves is conspicuous.

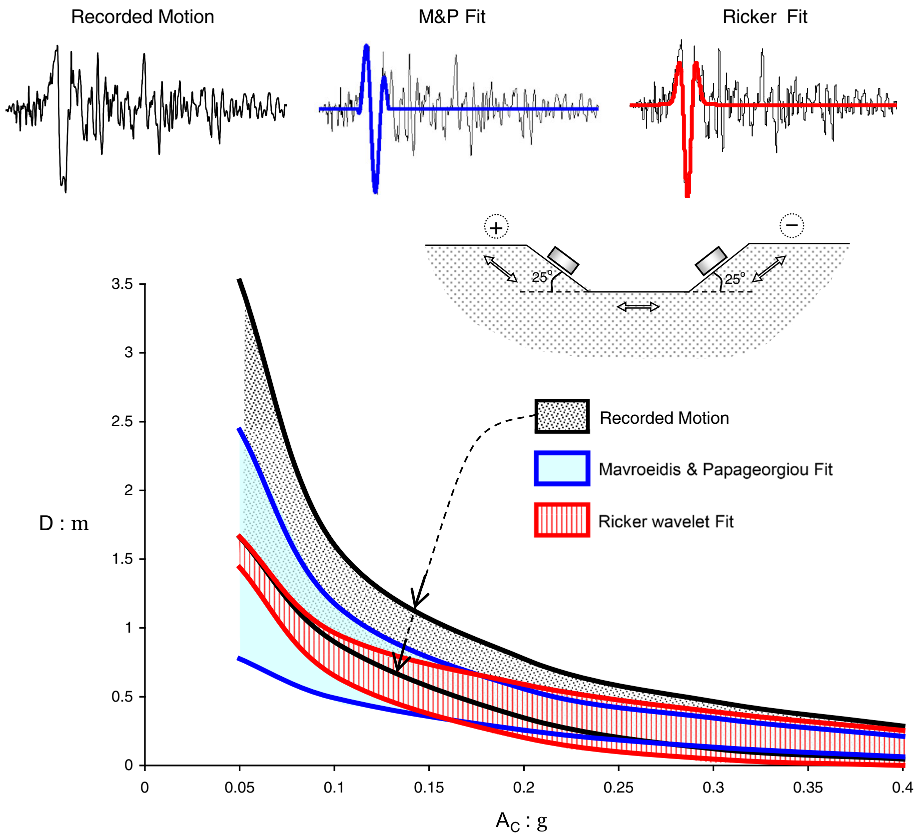

Fig. 12 Sliding spectra triggered by the Rinaldi 228° record, imposed with both polarities (hence, two curves per motion). Comparison with the slippage response to the corresponding fitted Ricker and M&P wavelets. The *shading* between each pair of curves with the *same color* is used only for visualizing the difference in response due to changing polarity from + to −

Another simple but revealing example of the importance of polarity on asymmetric sliding is portrayed in Fig. 13. The TCU 068-NS record (1999 Chi-Chi) is the excitation. Figure 13 illustrates the slippage time-histories in response to the original record and the two fitted wavelets. First, regarding the acceleration histories: the 'flinged' record of TCU 068-NS (PGA ≈ 0.35 g) is approximated with a long period M&P wavelet (PGA ≈ 0.13 g, merely one-third of the PGA) and with a high frequency Ricker wavelet (PGA ≈ 0.30 g, near the true PGA). In other words, the TCU 068 accelerogram is approached by two "opposite" perspectives in terms of frequency content. The response shows that it is the long period M&P wavelet that comes much closer to reality (although not close enough), as summarized in the sliding spectra of Fig. 14. Evidently, the Ricker wavelet misses completely the huge impulse $\Delta V \times \tau$ (where τ is the pulse duration) of the record between about 3–10 s.

A summary of all the numerical analyses performed in this study for the symmetric and asymmetric sliding is displayed in Fig. 14. Sliding spectra for inclination angle $\beta = 25°$ are plotted without reversing polarity for the sake of clarity. Notice that the in some of the records the sliding response is in reasonable agreement with the corresponding wavelet sliding spectra, but in several others the deviation ranges from moderate to huge.

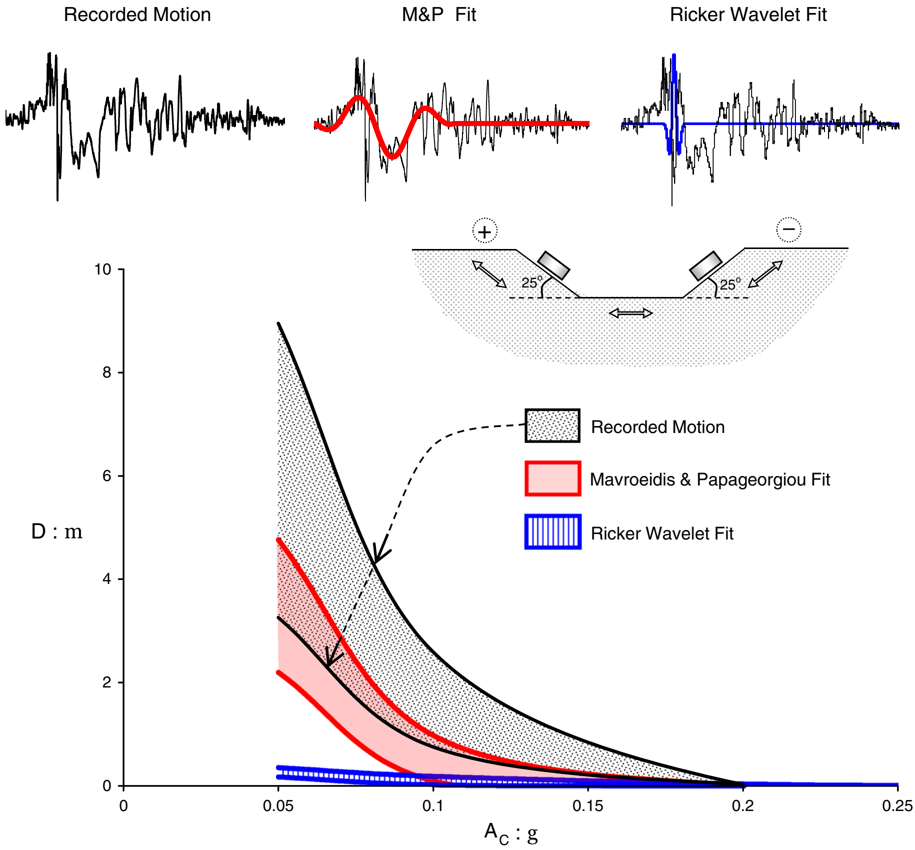

Fig. 13 Sliding spectra triggered by the TCU 068-NS ground motion, imposed with both polarities (hence, two curves per motion). Comparison with the slippage response of the corresponding Ricker and M&P wavelet fit to the real accelerogram of Chi-Chi

6 Compilation of results and the pulse indicator

The pulse indicator, *pI*, is an index introduced by Vassiliou and Makris (2011): a qualitative and quantitative measure of a wavelet's similarity to a record, and its ability to retain the most destructive features of the record. Pulse indicator, *pI*, is defined as:

$$pI = \frac{1}{2}\left(e_a + e_v\right) \tag{5}$$

where e_a is a measure used to evaluate the capability of a wavelet to locally match the predominant acceleration pulse of the accelerogram A(t):

$$e_a = \frac{\int_{-\infty}^{\infty} A(t) \cdot \lambda\left(s, \xi\right) \cdot \psi(t) dt}{\int_{-\infty}^{\infty} A^2(t) dt} \tag{6}$$

and e_v is the corresponding velocity ratio, defined as:

$$e_v = \frac{\int_{-\infty}^{\infty} V(t) \cdot \upsilon(t) dt}{\int_{-\infty}^{\infty} V^2(t) dt} \tag{7}$$

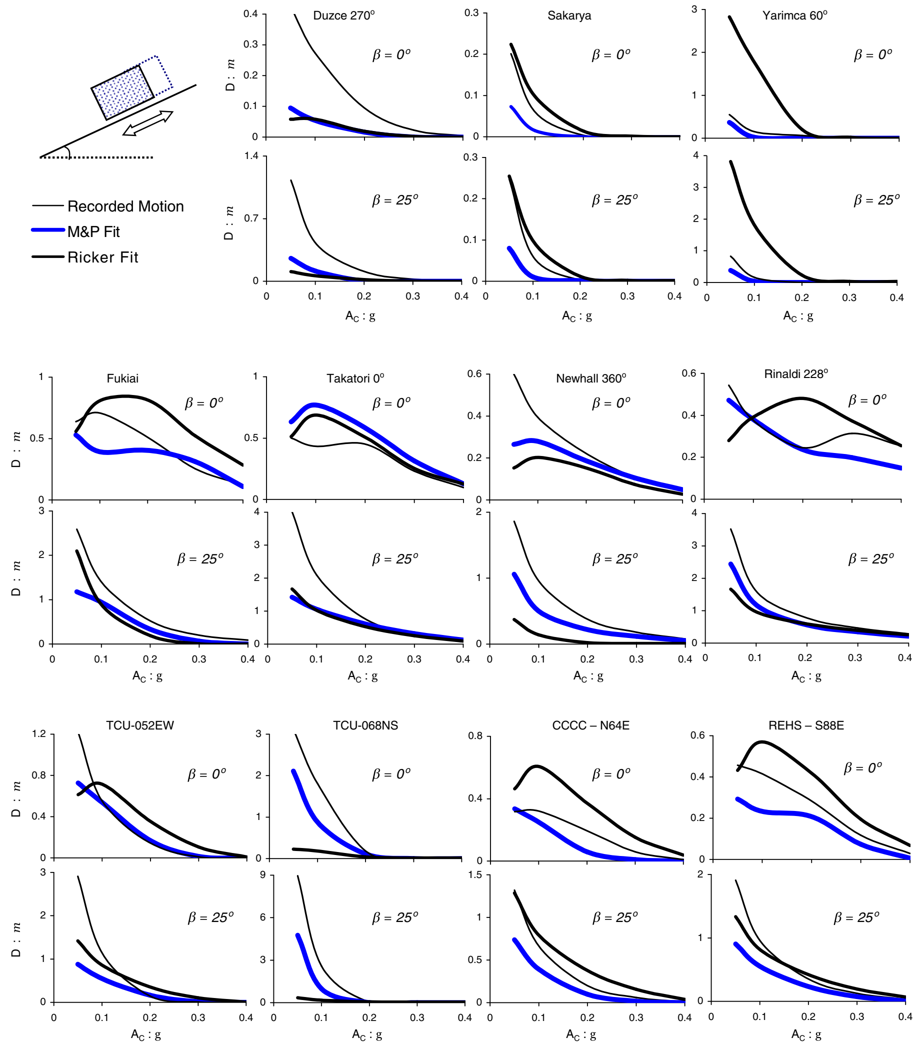

Fig. 14 Sliding spectra, D, of a rigid block yielding with critical acceleration, A_C, on top of a *horizontal* or *inclined plane*. With the *bold black line* is illustrated the response triggered by the Ricker fitted wavelet, whereas with the *bold grey line* the response of the M&P wavelet fit. Both are compared with the acceleration response induced by the original record

where $V(t)$ is the recorded ground velocity time-history, and υ(t) is the velocity pulse of the matching wavelet acceleration pulse. The remaining symbols have been defined after Eqs. 1–4.

Table 2 lists the values of the acceleration matching index, $e_{a,}$ velocity matching index, e_υ, and pulse indicator, *pI*, for the 11 records of our study. A few important observations can be made: First, for a record whose fitted wavelet produces large (>0.30) values for both e_a and e_υ, the wavelet-induced sliding displacements are in close agreement with those of the original record. For example, the Fukiai record for which the Ricker and the M&P wavelets achieve e_a and e_υ values that are both greater than 0.40. In fact, if a wavelet approximates the most significant features of a record successfully, it will display e_a and e_υ values larger than

Table 2 Acceleration matching index, e_a, velocity matching index, e_V, and the pulse indicator, *pI*, for each record

Record name	M&P wavelet			Ricker wavelet		
	e_a	e_V	*pI*	e_a	e_V	*pI*
Fukiai	0.44	0.54	0.49	0.44	0.66	0.55
Takatori-0°	0.34	0.46	0.40	0.28	0.37	0.33
Newhall Firestation-360°	0.40	0.34	0.37	0.25	0.19	0.22
Rinaldi-228°	0.49	0.67	0.58	0.49	0.61	0.55
TCU 052-*EW*	0.62	0.07	0.35	0.68	0.09	0.38
TCU 068-*NS*	0.34	0.69	0.51	0.16	0	0.08
Sakarya-EW	0.10	0.06	0.08	0.13	0.05	0.09
Yarimca-60°	0.22	0.52	0.37	0.42	0.87	0.64
Duzce-270°	0.20	0.05	0.13	0.13	0.02	0.07
CCCC-N64E	0.44	0.45	0.44	0.48	0.54	0.51
REHS-S88E	0.54	0.41	0.47	0.48	0.48	0.48

The fitted pulse can be either a Ricker or a M&P wavelet

0.30–0.40 (Vassiliou and Makris 2011). Second, only a large acceleration index, e_a, is not an indicator of a wavelet that can adequately describe the sliding response. For instance, with the TCU 052-EW record the fitted M&P wavelet achieves a substantial acceleration index $e_a = 0.62$ but the velocity index is extremely low ($e_v = 0.07 << 0.4$). And indeed, as has been shown earlier, sliding due to the actual record deviates substantially from that due to the wavelet.

To visualize better the above, Figs. 15 and 16 depict for symmetric and asymmetric sliding respectfully the ratio of the wavelet triggered slippage, $D_{M\&P}$ or D_{RICKER}, divided by the real sliding displacement D, as functions of the critical sliding acceleration A_C. If a wavelet triggered slippage coincided with the actual, the aforementioned slippage ratio would be unity: a perfect agreement. Now, for sliding on horizontal plane, notice in Fig. 15a that the induced slippage of the Rinaldi record (shown with triangles) is very similar with the slippage due to M&P wavelet; with pulse indicator $pI = 0.58$, the largest of all cases ! Notice that the sliding response ratio, $D_{M\&P}$/D, is very close to unity for all A_C values. Naturally the agreement seams not so perfect with asymmetric sliding (Fig. 16), where the Rinaldi $D_{M\&P}$/D ratio is about 0.75 (with *pI* of course remaining 0.58). That is obviously a shortcoming of the pulse index definition: it can not distinguish the response on horizontal and inclined plane; hence pI can not capture the effects of reversing polarity. On the contrary, the Düzce approximation results to small values of $D_{M\&P}$/D (solid squares) in accord with their poor pulse indicator, $pI = 0.13$. Additional observations can be readily made from the plots of Figs. 15 and 16.

To sum up, the pulse indicator (Eqs 5-7) seems to be a reasonable and successful measure of the wavelet matching process, not only for elastic systems but also for the strongly inelastic and even strongly asymmetric systems.

7 Summary and conclusions

Earthquake response of four fundamental analogues, representative of a wide variety of structural, geotechnical, and geological systems, have been subjected to several near-fault ground motions and two fitted wavelets, the M&P and Ricker.

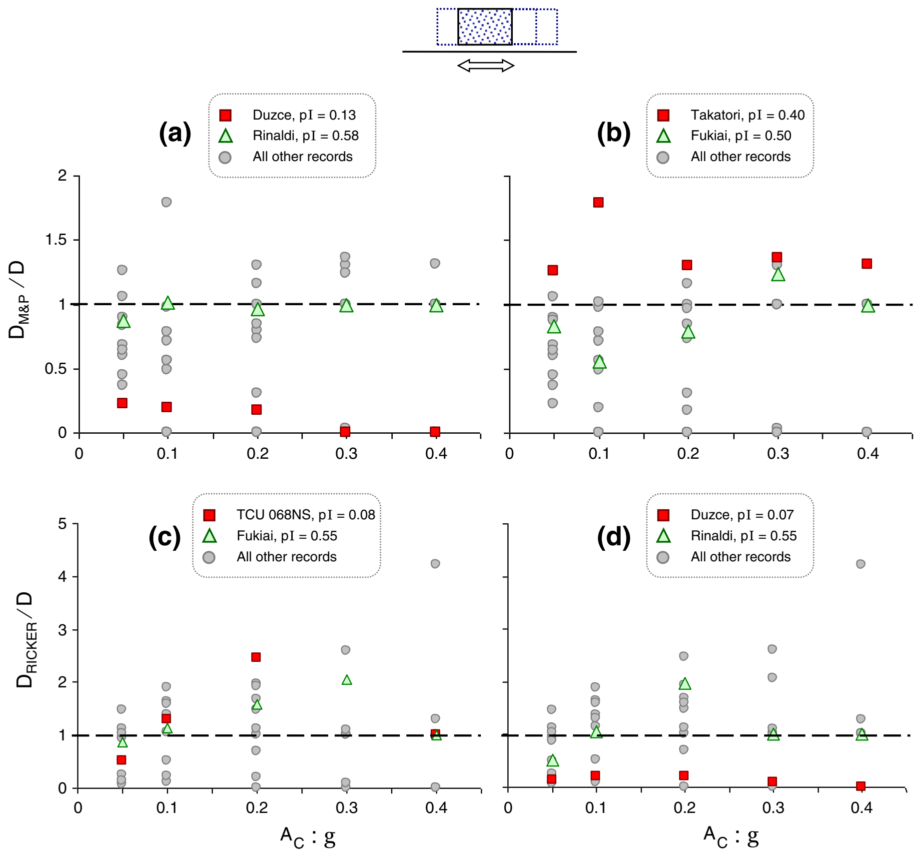

Fig. 15 Summary of results for the symmetric sliding displacement, D, induced by an original recorded motion normalized by the slippage triggered by: (i) the fitted M&P wavelet, $D_{M\&P}$, and (ii) the Ricker fitted wavelet, D_{RICKER}.

Forward-rupture directivity and fling-step affected near-fault motions, containing ‘severe’ acceleration pulses and/or large velocity steps, have been shown to lead to strong response of elastic and merely of inelastic systems. Sliding systems being of rigid-plastic nature without elasticity, may experience a profound and unpredictable slippage from such motions, especially if their “strength” (critical yielding acceleration or coefficient of friction) is small. Most interesting, changing the polarity of such an excitation may have a dramatic effect on the accumulating slip. This is a conclusion that should be recalled in field post-earthquake reconnaissance, when trying to explain different degrees of damage suffered by similar man-made or natural “structures” in close proximity to one another but with different orientation.

Comparison between the response to actual records and the response to the fitted wavelets has shown that whereas the elastic response is not very sensitive to the motion details and the wavelet approximation is thus satisfactory, sliding systems are quite sensitive not only to the exact pulse-like characteristics retained in a fitted wavelet, but also to the detailed sequence of pulses and the number of accelerogram’s cycles. The pulse indicator (introduced by Vassiliou and Makris 2011) seems to be an efficient measure of the matching wavelet ability, even for sliding systems.

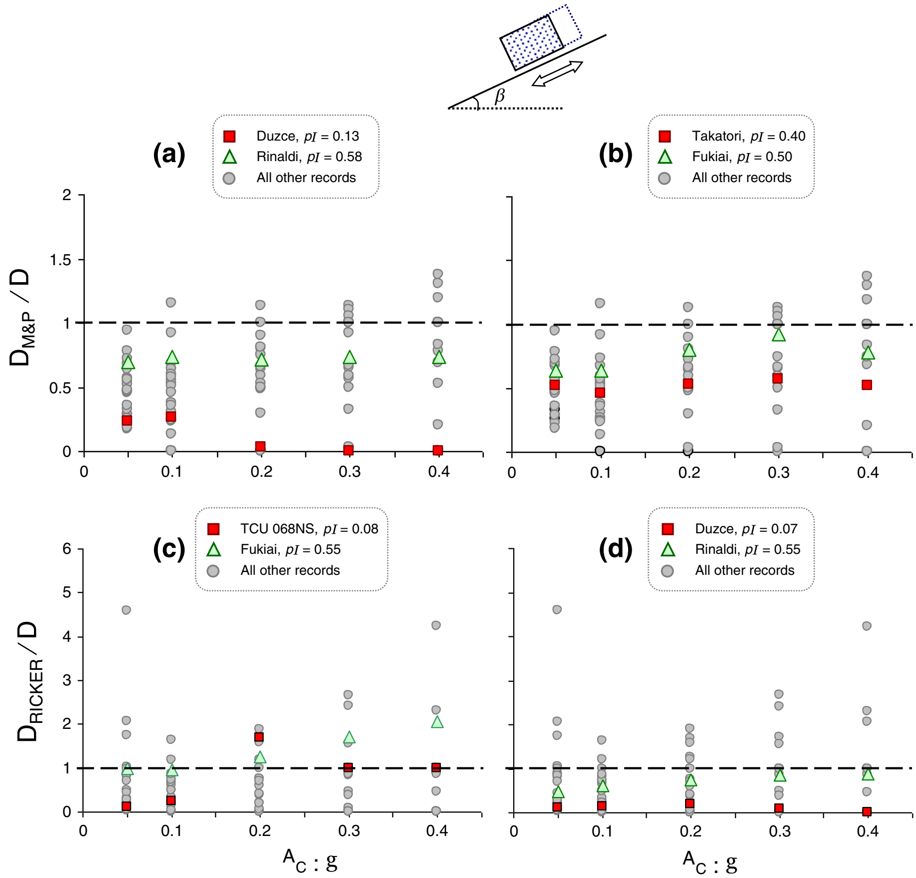

Fig. 16 Summary of results for the asymmetric sliding displacement, D, induced by an original recorded motion normalized by the slippage triggered by: (i) the fitted M&P wavelet, $D_{M\&P}$, and (ii) the Ricker fitted wavelet, D_{RICKER}.

Acknowledgments The work of this paper was conducted for the project "DARE", financed by a European Research Council (ERC) under the "Ideas" Advanced Grant Programme in Support of Frontier Research [Grant Number ERC-2-9-AdG228254-DARE]. The authors would like to thank the doctoral student *Georgios Kampas* for his kind help in deriving the wavelets needed in the paper. We also acknowledge the two anonymous Reviewers for their thoughtful comments and suggestions.

References

Abrahamson NA (2000) Effects of rupture directivity on probabilistic seismic hazard analysis. In: Proceedings, 6th international conference on seismic zonation, palm springs, California, Earthquake Engineering Research Institute

Abrahamson NA (2001) Incorporating effects of near fault tectonic deformation into design ground motions, University at Buffalo MCEER: Friedman F. V. Professional Program, webcast, http://mceer.buffalo.edu/outreach/pr/Abrahamson.asp

Ambraseys NN, Sarma SK (1967) The response of earth dams to strong earthquakes. Géotechnique 17:181–213

Ambraseys NN, Menu J (1988) Earthquake induced ground displacements. Earthq Eng Struct Dyn 16:985–1006

Bertero VV, Mahin SA, Herrera RA (1978) Aseismic design implications of near-fault San Fernando earthquake records. Earthq Eng Struct Dyn 6:31–42
Bolt BA (1976) Abnormal seismology. Bull Seismol Soc Am 66:617–623
Bolt BA (2004) Earthquakes, 5th edn. W. H. Freeman & Co, New York
Bray JD, Rathje EM (1998) Earthquake-induced displacements of solid-waste landfills. J Geotech Geoenviron Eng ASCE 124:242–253
Constantinou MC and Gazetas G (1987) Probabilistic seismic sliding deformations of earth dams and slopes. In: Proceedings of the specialty conference on probabilistic mechanics and structural reliability, ASCE, Berkeley, pp 318–321
Constantinou MC, Gazetas G, Tadjbakhsh I (1984) Stochastic seismic sliding of rigid mass supported through non-symmetric friction. Earthq Eng Struct Dyn 12:777–793
Crespellani T, Madiai C, Vannucchi G (1998) Earthquake destructiveness potential factor and slope stability. Geotechnique 48:411–420
Fenves G, Chopra AK (1986) Simplified analysis for earthquake resistant design of concrete gravity dams. Report UBC/EERC-85/10. University of California, Berkeley
Garini E, Gazetas G, Anastasopoulos I (2011) Asymmetric 'Newmark' sliding caused by motions containing severe 'directivity' and 'fling' pulses. Géotechnique 61(9):733–756
Gazetas G, Garini E, Anastasopoulos I, Georgarakos T (2009) Effects of near-fault ground shaking on sliding systems. J Geotech Geoenviron Eng ASCE 135(12):1906–1921
Gazetas G, Uddin N (1994) Permanent deformation on pre-existing sliding surfaces in dams. J Geotech Eng ASCE 120(11):2041–2061
Harp EL, Jibson RW (1995) Seismic instrumentation of landslides: building a better model of dynamic landslide behaviour. Bull Seismol Soc Am 85:93–99
Hisada Y, Bielak J (2003) A theoretical method for computing near-fault ground motions in layered half-spaces considering static offset due to surface faulting, with a physical interpretation of fling step and rupture directivity. Bull Seismol Soc Am 93(3):1154–1168
Karavasilis TL, Makris N, Bazeos N, Beskos DE (2010) Dimensional response analysis of multi-storey regular steel MRF subjected to pulse-like earthquake ground motions. J Struct Eng ASCE 136(8):921–932
Kramer SL (1996) Geotechnical earthquake engineering. Prentice-Hall, Englewood Cliffs
Kramer SL, Smith M (1997) Modified Newmark model for seismic displacements of compliant slopes. J Geotech Geoenviron Eng ASCE 123:635–644
Leger P, Katsouli M (1989) Seismic stability of concrete gravity dams. Earthq Eng Struct Dyn 18:889–902
Lin JS, Whitman RV (1983) Decoupling approximation to the evaluation of earthquake-induced plastic slip in earth dams. J Geotech Eng Div ASCE 11:667–678
Makdisi FI, Seed HB (1978) Simplified procedure for estimating dam and embankment earthquake induced deformations. J Geotech Eng Div ASCE 104:849–867
Makris N and Black CJ (2004a) Dimensional analysis of rigid-plastic and elastoplastic structures under pulse-type excitations. J Eng Mech ASCE 130(9):1006–1018
Makris N and Black CJ (2004b) Dimensional analysis of bilinear oscillators under pulse-type excitations. J Eng Mech, ASCE 130(9):1019–1031
Makris N and Black CJ (2004c) Evaluation of peak ground velocity as a "good" intensity measure for near-source ground motions. J Eng Mech ASCE 130(9):1032–1044
Makris N, Psychogios T (2006) Dimensional response analysis of yielding structures. Earthq Eng Struct Dyn 35:1203–1224
Mavroeidis PG, Papageorgiou SA (2003) A mathematical representation of near-fault ground motions. Bull Seismol Soc Am 93(3):1099–1131
Mavroeidis PG, Papageorgiou SA (2010) Effect of fault rupture characteristics on near-fault strong ground motions. Bull Seismol Soc Am 100(1):37–58
Newmark NM (1965) Effects of earthquakes on dams and embankments. Géotechnique 15(2):139–160
Rathje EM, Bray JD (1999) An examination of simplified earthquake-induced displacement procedures for earth structures. Can Geotech J 36:72–87
Richards R, Elms DG (1979) Seismic behaviour of gravity retaining walls. J Geotech Eng Div ASCE 105:449–464
Sarma SK (1975) Seismic stability of earth dams and embankments. Géotechnique 25(4):743–761
Sarma SK (1981) Seismic displacement analysis of earth dams. J Geotech Eng Div ASCE 107:1735–1739
Sarma SK and Kourkoulis R (2004) Investigation into the prediction of sliding block displacements in seismic analysis of earth dams. In: Proceedings of the 13th world conference on earthquake engineering, Vancouver, Canada, paper no 1957
Singh JP (1985) Earthquake ground motions: implications for designing structures and reconciling structural damage. Earthq Spectra 1:239–270

Somerville P (2000) Seismic hazard evaluation, 12th WCEE 2000, Bulleting of the New Zealand Society of Earthquake Engineering, vol 33, pp 325–346 and 484–491

Somerville P (2003) Characterization of near fault ground motions for design, ACI specialty conference, U.C. San Diego, American Concrete Institute

Somerville PG, Saikia C, Wald D, Graves R (1996) Implications of the Northridge earthquake for strong ground motions from thrust faults. Bull Seismol Soc Am 86:115–125

Somerville PG, Smith NF, Graves RW, Abrahamson NA (1997) Modification of empirical strong ground motion attenuation relations to include the amplitude and duration effects of rupture directivity. Seismol Res Lett 68:199–222

Vassiliou MF and Makris N (2009) Evaluation of the coherence of ground motions and their effect on the seismic demand of structures. In: Proceedings of the ACES workshop: advances in performance-based earthquake engineering, Corfu, Greece

Vassiliou MF, Makris N (2011) Estimating time scales and length scales in pulselike earthquake acceleration records with wavelet analysis. Bull Seismol Soc Am 101(2):596–618

Wilson RC, Keefer DK (1983) Dynamic analysis of a slope failure from the 6 August, 1979 Coyote Lake, California Earthquake. Bull Seismol Soc Am 73(3):863–877

Yegian MK, Marciano EA, Ghahraman VG (1991) Earthquake induced permanent deformations: a probabilistic approach. J Geotech Eng ASCE 117:35–50

Yegian MK, Harb JN, Kadakal U (1998) Dynamic response analysis procedure for landfills and geosynthetic liners. J Geotech Geoenviron Eng ASCE 124(10):1027–1033